



**HAL**  
open science

## About the use of $^{13}\text{C}$ - $^{13}\text{C}$ NOESY in bioinorganic chemistry

V. Ghini, Soizic Chevance, P. Turano

► **To cite this version:**

V. Ghini, Soizic Chevance, P. Turano. About the use of  $^{13}\text{C}$ - $^{13}\text{C}$  NOESY in bioinorganic chemistry. *Journal of Inorganic Biochemistry*, 2019, 192, pp.25-32. 10.1016/j.jinorgbio.2018.12.006 . hal-02043063

**HAL Id: hal-02043063**

**<https://univ-rennes.hal.science/hal-02043063>**

Submitted on 9 Jul 2020

**HAL** is a multi-disciplinary open access archive for the deposit and dissemination of scientific research documents, whether they are published or not. The documents may come from teaching and research institutions in France or abroad, or from public or private research centers.

L'archive ouverte pluridisciplinaire **HAL**, est destinée au dépôt et à la diffusion de documents scientifiques de niveau recherche, publiés ou non, émanant des établissements d'enseignement et de recherche français ou étrangers, des laboratoires publics ou privés.



Distributed under a Creative Commons Attribution - NonCommercial - NoDerivatives 4.0 International License



## Focused review

About the use of  $^{13}\text{C}$ - $^{13}\text{C}$  NOESY in bioinorganic chemistryVeronica Ghini<sup>a</sup>, Soizic Chevance<sup>a,b</sup>, Paola Turano<sup>a,c,\*</sup><sup>a</sup> CERM, University of Florence, Via Luigi Sacconi 6, 50019 Sesto Fiorentino, Florence, Italy<sup>b</sup> Univ Rennes, CNRS, ISCR-UMR6226, SCANMat-UMS2001, F-35000 Rennes, France<sup>c</sup> Department of Chemistry "Ugo Schiff", University of Florence Via della Lastruccia 3, 50019 Sesto Fiorentino, Florence, Italy

## A B S T R A C T

Herein we present examples of the application of the  $^{13}\text{C}$ - $^{13}\text{C}$  Nuclear Overhauser Effect Spectroscopy (NOESY) experiment to the study of metalloproteins and we critically discuss the advantages and drawbacks of the method as a function of the molecular size of the investigated systems. The contribution is focused on a few case studies among the systems analyzed in the group of the corresponding author. The  $^{13}\text{C}$ - $^{13}\text{C}$  NOESY experiment represents the gold standard for the observation of NMR signals in the 480 kDa ferritin nanocage and for monitoring its interaction with iron. By decreasing the protein size, the experiment progressively loses its importance as a tool for the detection of the complete spin pattern of the amino acid side chains, as exemplified by nickel-dependent regulatory protein, NikR (molecular mass of the homo-tetramer  $\sim 80$  kDa). In very small proteins, such as mitochondrial cytochrome *c* (12.3 kDa), we are only able to detect cross peaks between adjacent  $^{13}\text{C}$  nuclei; this feature turned out to be useful for the assignment of the  $^{13}\text{C}$  core resonances of the porphyrin in a uniformly enriched heme.

## 1. Introduction

The present contribution is based on the lectures given by P. Turano at the Summer School of Bioinorganic Medicinal Chemistry held in August 2017, to which this Special Issue is dedicated. Among the several topics covered during those lectures, the present minireview focuses on some demonstrators of the potentialities of  $^{13}\text{C}$ - $^{13}\text{C}$  Nuclear Overhauser Effect Spectroscopy (NOESY) experiment in systems of different molecular size.

1.1. Why  $^{13}\text{C}$ -direct detection?

Biological NMR is largely based on  $^1\text{H}$  detection because of the highest sensitivity of this nucleus that stems from a high natural abundance (99.98%) and high gyromagnetic ratio ( $\gamma = 26.752 \cdot 10^7 \text{ rad s}^{-1} \text{ T}^{-1}$ ). Nevertheless, this approach shows its weak spot when one needs to deal with systems characterized by fast nuclear relaxation, as it occurs for paramagnetic species, where both longitudinal and transverse relaxation times ( $T_1$  and  $T_2$ , respectively) can be extremely short [1–4], or in large macromolecular assemblies where  $T_2$  decreases as the rotational correlation time  $\tau_c$  determined by molecular tumbling increases (Fig. 1). These effects are attenuated when passing to low  $\gamma$  nuclei such as  $^{13}\text{C}$  ( $\gamma = 6.728 \cdot 10^7 \text{ rad s}^{-1} \text{ T}^{-1}$ ). Given the dependence of relaxation rates ( $T_1^{-2}$  and  $T_2^{-1}$ ) on the  $\gamma^2$  of the involved nuclei, the advantage of using low  $\gamma$  nuclei for fast-relaxing systems becomes apparent. Of course, the low natural abundance of the  $^{13}\text{C}$  isotope needs to be counterbalanced by the use of uniform  $^{13}\text{C}$ -

labeling of protein samples. On the other hand, as a drawback of the low  $\gamma$ ,  $^{13}\text{C}$ -direct detection suffers for low sensitivity; the problem is attenuated by using dedicated probeheads for high magnetic field spectrometers. The development of the hardware has been flanked by the design of a complete set of protonless NMR experiments for the systematic assignment of protein backbone and side chains [5,6], based on exploiting the heteronuclear scalar correlations. This approach has been proposed initially by Bertini et al. for systems characterized by short relaxation times such large proteins and paramagnetic metalloproteins [7–10]. These experiments represent an alternative assignment strategy with respect to the sequences developed by Wüthrich and coworkers to obtain  $^{15}\text{N}$ - $^1\text{H}$  correlations in large macromolecular or supermolecular assemblies [11,12], which optimize transverse relaxation based on cross-correlated relaxation between dipole-dipole interactions and chemical shift anisotropy (CSA), and include transverse relaxation-optimized spectroscopy (TROSY), cross-correlated relaxation-enhanced polarization transfer (CRINEPT), and cross-correlated relaxation-induced polarization transfer (CRIPT).

## 1.2. Why NOESY?

In parallel to the above protonless experiments based on scalar correlations, the same authors proposed the use of heteronuclear dipolar correlations via  $^{13}\text{C}$ - $^{13}\text{C}$  NOESY [13] taking as test cases monomeric and dimeric superoxide dismutase (16 and 32 kDa, respectively). The gain in intensity when passing from the monomer to the dimer can be easily interpreted by recalling that Nuclear Overhauser effect (NOE)

\* Corresponding author at: CERM, University of Florence, Via Luigi Sacconi 6, 50019 Sesto Fiorentino, Florence, Italy.  
E-mail address: [turano@cerm.unifi.it](mailto:turano@cerm.unifi.it) (P. Turano).

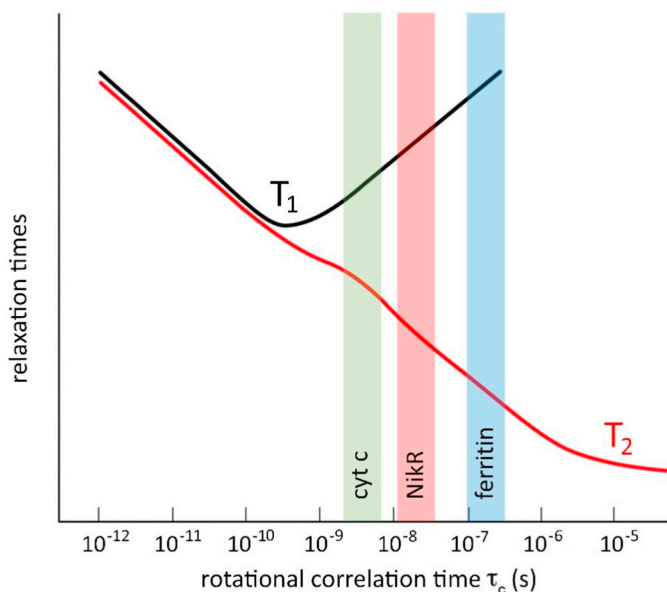


**Fig. 1.** Qualitative dependence of longitudinal,  $T_1$ , and transverse,  $T_2$ , nuclear relaxation times on the value of the rotational correlation time,  $\tau_c$ . For macromolecular systems,  $T_1$  and  $T_2$  values diverge, with the latter continuously decreasing and the former increasing. The colored areas represent those of relevance for the examples discussed in this contribution, namely *Rana catesbeiana* H' ferritin (blue), *Helicobacter pylori* nickel-dependent regulatory protein NikR (red), and human cytochrome c, cyt c (green).

varies proportionally with  $T_1$  and the rotational correlation time  $\tau_c$ . For a rigid molecule, the latter increases with molecular size, as roughly deducible from the Stokes-Einstein relationship. As qualitatively depicted in Fig. 1, for macromolecules  $T_1$  in turn increases with increasing  $\tau_c$ , while the transverse relaxation time  $T_2$  decreases.

Therefore, depending on where the investigated system settles along the  $\tau_c$  axis, the use of  $^{13}\text{C}$ - $^{13}\text{C}$  NOESY might become particularly favorable. On the other hand, the continuous decrease in  $T_2$  results as progressively detrimental for the detection of scalar correlations. In Section 2 we present three examples of largely different size and  $\tau_c$ , and we discuss the advantages and disadvantages of the use of dipolar vs. scalar correlations.

## 2. $^{13}\text{C}$ - $^{13}\text{C}$ NOESY: examples of application to metalloproteins

### 2.1. Ferritin

The so-called maxiferritins are nanocage proteins of molecular mass of the order of 500 kDa that self-assemble from 4-helix bundle subunits to form a hollow structure of spherical shape, with an external diameter of 12 nm; the internal cavity, designed to host a ferric oxo biominer, has a diameter of about 8 nm (Fig. 2A). The structure is highly symmetric (O symmetry) with C2, C3 and C4 symmetry axes respectively along the contacts between antiparallel-oriented pairs of subunits, along the channels that form where three subunits from different pairs come in contact, and along the channels where the four subunits from different pairs come in contact (Fig. 2A) [14]. As reviewed elsewhere, the symmetry properties of the cage represent an obvious simplification for the NMR analysis when dealing with homopolymeric ferritin cages, where the number of detectable signals equals that expected for a single subunit [15].

On the other hand, the overall molecular size is an obvious drawback. From nuclear magnetic resonance dispersion (NMRD) measurements we estimated  $\tau_c$  values from 135 ns at 298 K, down to 85 ns at 328 K. The coherence transfer at the basis of experiments relying on scalar couplings severely suffers for the reduced transverse relaxation

times in ferritin. In practice, all the coherence-transfer protonless experiments failed to provide detectable signals due to severe transverse relaxation during coherence transfer steps. The CRINEPT-TROSY, which in our hands was a successful experiment for the study of protein assemblies of apparent size of the order of 150 kDa [16], in the case of H' ferritin allowed us the detection of only a fraction of the expected  $^1\text{H}$ - $^{15}\text{N}$  signals, even when operating at relatively high temperatures to speed up molecular tumbling, and using perdeuterated samples to attenuate the relaxation via coupling with  $^1\text{H}$ . Protein perdeuteration, to diminish the density of protons, eliminates many of the spin-diffusion relaxation pathways, thus reducing the efficiency of  $^1\text{H}$  relaxation. Additionally, because of the smaller gyromagnetic ratio of deuterium ( $\gamma = 4.11 \cdot 10^7 \text{ rad s}^{-1} \text{ T}^{-1}$ ) with respect to proton, the relaxation times of the  $^{13}\text{C}$  and  $^{15}\text{N}$  spins are greatly increased [17]. As far as the effect of temperature on the correlation time is concerned, it is worth noting that, even in a highly thermostable protein like ferritin, long-lasting experiments at very high temperature are not easily feasible due to at least partial structure destabilization/unfolding (as observed for ferritin pores around 325–330 K) [18]; moreover, 323 K is an upper-limit operating temperature for cryoprobes.

On the contrary, in the  $^{13}\text{C}$ - $^{13}\text{C}$  NOESY maps intra-residue connectivities could be easily detected for most residues in the aliphatic region of the spectrum (Fig. 2B). At shorter mixing times the most intense peaks are those between carbon nuclei connected by a single bond. At longer mixing times, spin diffusion effects become operative and allow to draw the entire pattern of intra-chain connectivities, as illustrated in Fig. 2C for Ile and Val [19].

Nevertheless,  $^{13}\text{C}$ - $^{13}\text{C}$  NOESY as a stand-alone experiment does not allow the sequence specific assignment of the signals. Our attempts to push forward the limits of the technique aimed at observing long range inter-residue dipolar interactions failed. We therefore resorted to solid-state magic angle spinning (MAS) NMR on ferritin microcrystals, which provided the sequence specific assignment of 75% of the protein residues [20].

An important feature for the successful use of combined solution and solid-state NMR approaches is the possibility of a straightforward transfer of signal assignment from one state to the other. In the case of ferritin, the  $^{13}\text{C}$ - $^{13}\text{C}$  NOESY spectra are essentially superimposable with the  $^{13}\text{C}$ - $^{13}\text{C}$  correlated spectra obtained by solid-state NMR methods on microcrystalline samples produced by PEG precipitation [15,20] or on pelleted samples prepared by ultracentrifugation of concentrated protein solutions [20–23]. When corrected for the isotope effect on the chemical shift induced by the presence of  $^2\text{H}$  nuclei in the solution samples, the assignment of the aliphatic side chains could be automatically transferred. This was the starting point for our experiments aimed at monitoring the ferritin-assisted biomineralization.

In ferritin cages containing H or H'-type subunits the iron biomineralization is an enzymatically-assisted process, thanks to the presence of the so-called ferroxidase centers where iron(II) is oxidized to ferric species by oxygen. Because of this activity, the titration of ferritin solutions with iron(II) salts leads to a progressive increase in ferric species. The formation of ferric products was monitored via  $^{13}\text{C}$ - $^{13}\text{C}$  NOESY thanks to the paramagnetic-induced broadening beyond detection of the resonances of residues nearby the ferric products [15,20]. The paramagnetism of the ferric products was measured by the Evans method and suggested the formation of ferric clusters of increasing nuclearity characterized by antiferromagnetic coupling. In a protein of this size at 700 MHz, the paramagnetic transverse relaxation is dominated by the Curie relaxation [24] and therefore the broadening effects can be translated into distance limits: the signals of any nucleus within 5 Å from ferric ions are expected to be broadened beyond detection. On these bases, we suggested a location for the first binuclear species that forms at the ferroxidase site and a possible pathway for the ferric clusters that form during subsequent catalytic turnovers [15,20]. These NMR results inspired the development of time-lapse anomalous crystallography to characterize the ferroxidase center of ferritins. This

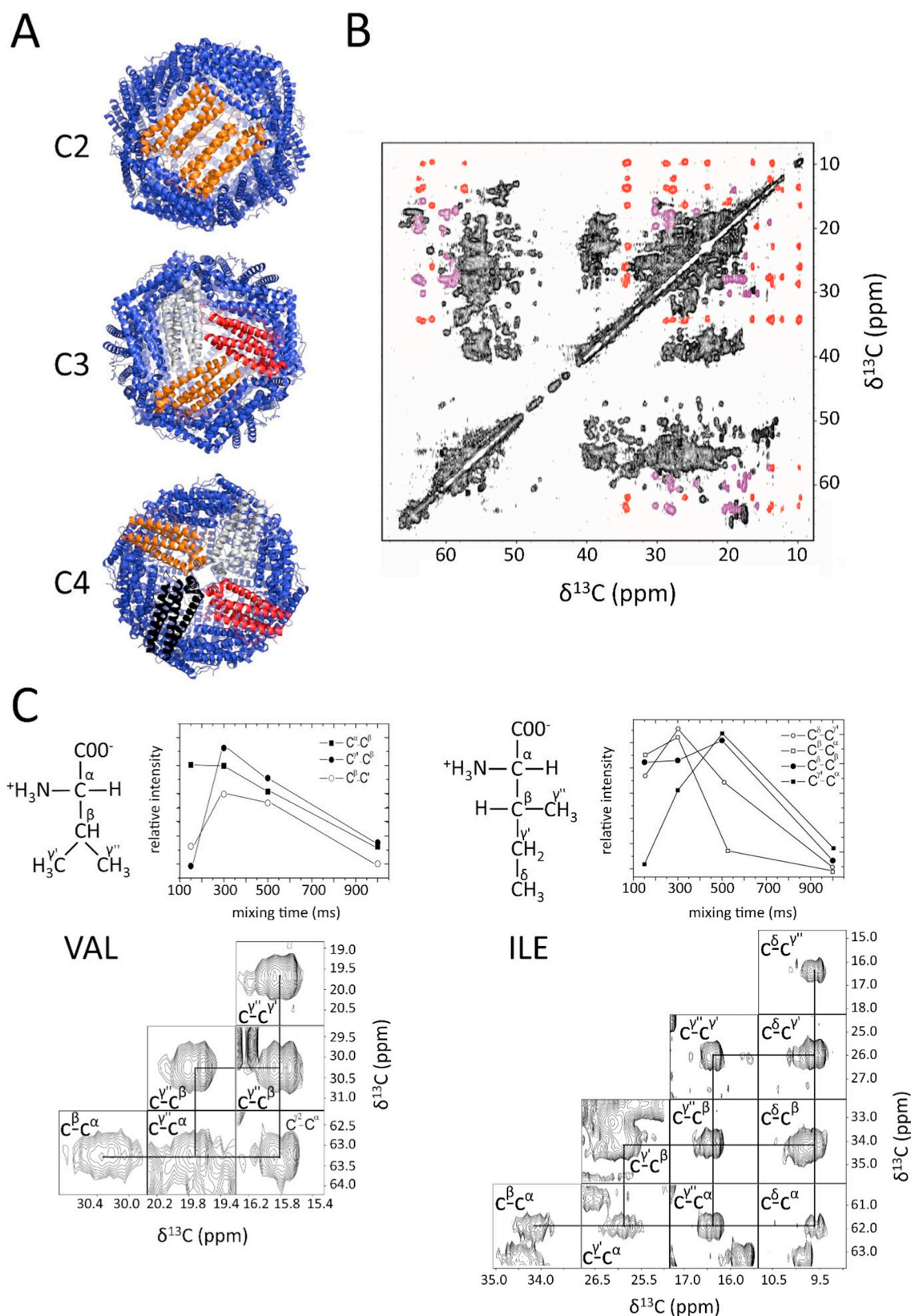


**Fig. 2.** (A) The nanocage structure of 24-mer ferritins is characterized by octahedral (432) symmetry. Along the 6 C2-symmetry axes, pairs of antiparallel-oriented subunits give rise to extensive intersubunit contacts. Groups of three symmetry-related subunits from different pairs form eight channels along the four C3 axes. Groups of four symmetry-related subunits from different pairs create the six channels along the 3 C4 axes. (B) The  $^{13}\text{C}$ - $^{13}\text{C}$  NOESY spectrum of homopolymeric perdeuterated H' ferritin from *Rana catesbeiana* recorded on a spectrometer operating at 700 MHz proton frequency and equipped with a triple-resonance TXO probe optimized for  $^{13}\text{C}$  direct detection experiments 500 ms mixing time at 298 K (total experiment time ~40 h). The signals of the side chains of Ile and Val residues are colored in red and violet, respectively. (C) NOESY pattern for Ile and Val residues and dependence of cross-peak intensities on mixing time for selected connectivities. Source: Panels (B) and (C) are adapted from [19].

method also provided a description of the iron(II) path from bulk solution to the inner cavity, via C3 channels, and then its assisted delivery to the ferroxidase centers [25–28]. Instead, clusters of high nuclearity have never been detected by X-ray crystallography although they have been proposed as biomineral precursors also on the basis of independent Mössbauer experiments [29–31]. Their evanescence in crystallography is probably because they are spatially disordered; a similar situation is encountered for the caged biomineral.

The example of the interaction of iron with H' ferritin extends the use of  $^{13}\text{C}$ - $^{13}\text{C}$  NOESY for the characterization of the protein interactome beyond the already proposed application in monitoring protein-protein surface contacts [32].

## 2.2. *Helicobacter pylori* nickel-dependent regulatory protein, NikR

The NikR protein is a nickel-dependent regulatory protein. In the gastric pathogen *Helicobacter pylori*, NikR regulates the expression of urease. NikR is a homotetrameric protein that belongs to the ribbon-helix-helix family of transcriptional regulators; the subunits (~20 kDa each) consist of two different domains: a N-terminal DNA-binding domain and a C-terminal domain that is required for nickel binding and for tetramerization. The two domains are connected by a flexible linker; as result, the homotetramer can adopt three overall conformations depending on the relative orientation of the DNA binding domains with respect to the central tetramerization core formed by the metal binding

domains, i.e. open, trans and cis conformations (Fig. 3A); the latter is stabilized by DNA binding [33].

S. Ciurli and P. Carloni performed atomistic and coarse-grained molecular dynamic simulations to analyze the interconversion among the three conformers and the role played by nickel in modulating the dynamic of these equilibria [34]. The contribution of our lab to this study consisted in the use of NMR spectra as a fingerprint tool to monitor the number of conformers present in solution for the apo and 4-Ni(II) bound forms. The number of peaks observed for the backbone and side chains in solution NMR data pointed to the presence either of a single symmetric conformation or an average ensemble of conformers interconverting on the submillisecond time scale. The dynamic analysis of the system is beyond the scope of this manuscript. Here we concentrate, instead, on the methodological aspects of the NMR approach.

The NikR homotetramer is about one-sixth in size with respect to the 24-mer ferritin (Fig. 1) [35]. With a molecule of this size we could successfully detect the entire set of  $^1\text{H}$ - $^{15}\text{N}$  correlation for backbone amides by using TROSY-heteronuclear single quantum correlation (HSQC) experiments in the temperature range between 298 and 315 K for a perdeuterated sample. In our hands this spectrum provided better results with respect to coherence transfer protonless analogues. The highest temperature was used to improve the spectral quality by exploiting the reduced rotational correlation time  $\tau_c$  of the system. For both apo and 4-Ni(II) NikR, the  $^1\text{H}$ - $^{15}\text{N}$  TROSY-HSQC spectra contained a number of peaks consistent with the number of amino acids in the

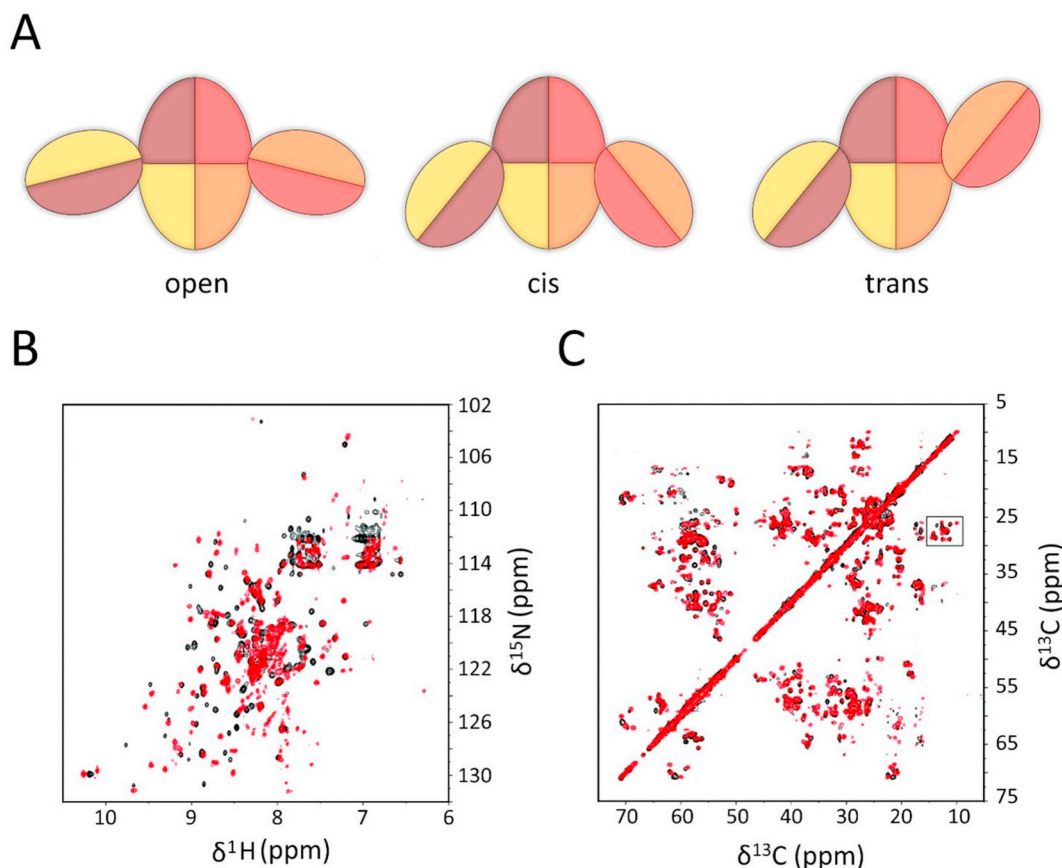


**Fig. 3.** (A) Schematic diagram of the open, cis and trans conformations of *H. pylori* NikR. Different colors identify different monomers, each constituted by a DNA binding and a metal binding domain. (B)  $^1\text{H}$ - $^{15}\text{N}$  TROSY-HSQC spectra of perdeuterated apo (black) and 4-Ni(II) (red) *H. pylori* NikR, recorded on a spectrometer operating at 700 MHz proton frequency at 315 K (C) The  $^{13}\text{C}$ - $^{13}\text{C}$  NOESY spectra of perdeuterated apo (black) and 4-Ni(II) (red) *H. pylori* NikR, recorded on a spectrometer operating at 700 MHz proton frequency and equipped with a triple-resonance TXO probe optimized for  $^{13}\text{C}$  direct detection experiments using 1.5 s mixing time at 315 K (total experiment time ~60 h). The of  $\text{C}\gamma_1$ - $\text{C}\delta$  cross-peaks for Ile residues are boxed; the dipolar connectivities between more distant carbons within the Ile side chains are barely visible (see Fig. 2C for comparison purposes). Source: The pictures of the NMR spectra are adapted from [34].

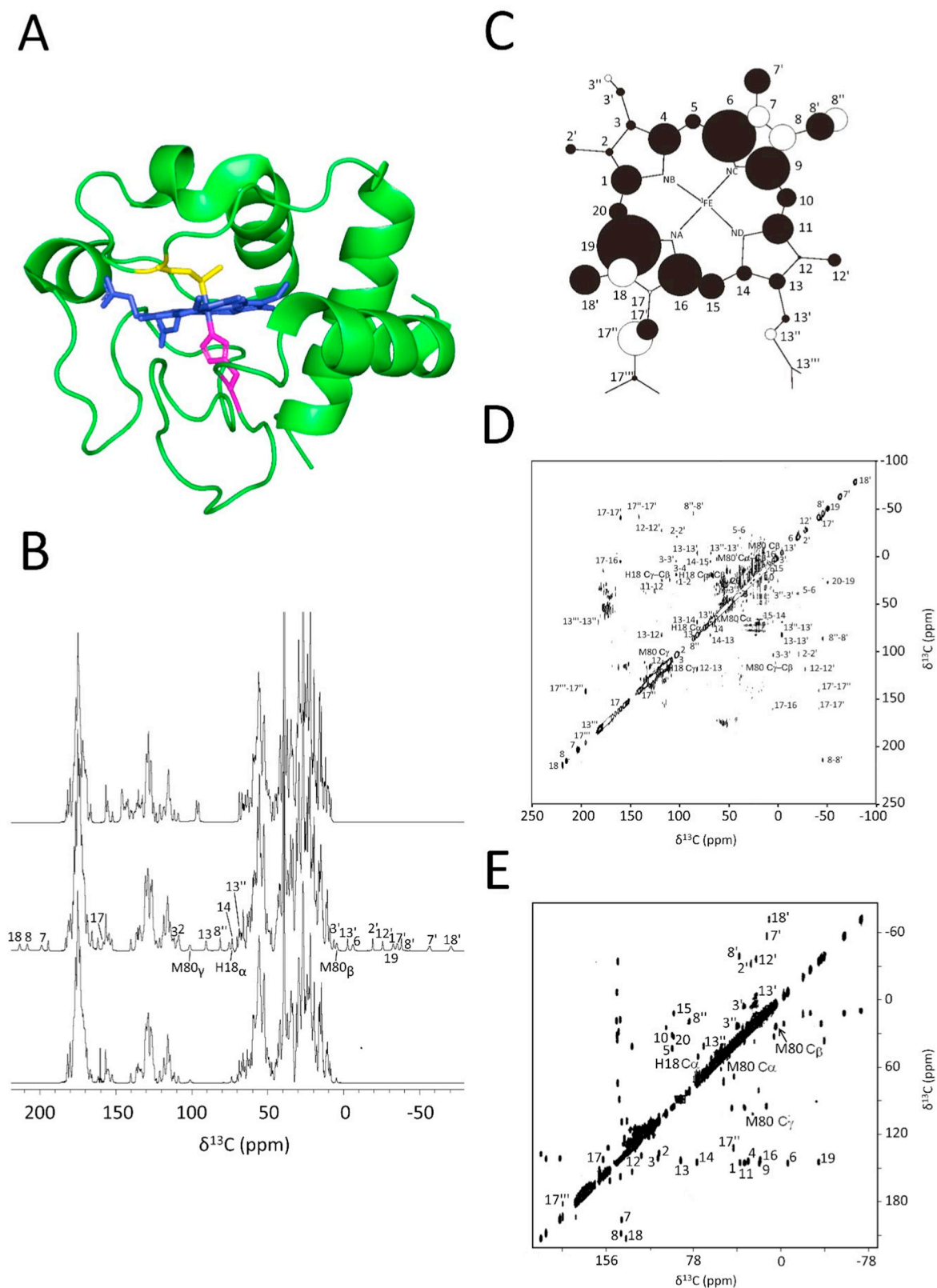


**Fig. 4.** (A) Ribbon representation of the structure of human cyt c; the heme and its axial ligands, His18 and Met80, are represented as blue, magenta and yellow sticks, respectively. (B)  $^{13}\text{C}$  one dimensional NMR spectra of fully  $^{13}\text{C}$ -enriched iron(II) (top), fully  $^{13}\text{C}$ -enriched iron(III) cyt c (middle); iron(III) cyt c with unlabeled heme (bottom). (C) Schematic representation of the heme and numbering of its carbon atoms. The circles represent the contact shift patterns for  $^{13}\text{C}$  nuclei (light grey circles for positive contact shifts; dark grey circles for negative contact shifts; the radius of each circle is proportional to the absolute value of the contact shift). (D)  $^{13}\text{C}$ - $^{13}\text{C}$  NOESY spectrum of fully  $^{13}\text{C}$ -enriched cyt c, acquired with 75 ms mixing time (total experiment time  $\sim 27$  h). (E)  $^{13}\text{C}$ - $^{13}\text{C}$  EXSY spectrum of fully  $^{13}\text{C}$ -enriched cyt c recorded, acquired with 35 ms mixing time (total experiment time  $\sim 15$  h); the sample contains a 3:1 mixture of the oxidized and reduced forms, for a total protein concentration of 2.9 mM. All spectra were recorded on a spectrometer operating at 700 MHz proton frequency and equipped with a triple-resonance TXO probe optimized for  $^{13}\text{C}$  direct detection experiments, at 300 K. Signal assignments follow the numbering of the scheme in panel C.

monomer (Fig. 3B); the observed differences in the pattern of chemical shift between the apo and holo forms reflect differences in backbone conformation induced by metal binding. It is worth mentioning that nickel binds to NikR in a squared-planar geometry and is therefore diamagnetic [36]. On the same samples,  $^{13}\text{C}$ - $^{13}\text{C}$  NOESY spectra were acquired to observe amino acid side chains. The smaller protein size with respect to ferritin implies shorter  $T_1$  and  $\tau_c$  values, and therefore a less efficient NOE. As a matter of fact, at variance to what reported for ferritin in Section 2.1 and Fig. 2, even with very long mixing times (up to 1.5 s) we could not detect the entire pattern of spins within amino acids side chains. The situation is clearly visible in Fig. 3C. Nevertheless, the spectral resolution allowed us to count the number of side chains and determine again a number of peaks that equals that expected for a symmetric homotetramer.

### 2.3. Mitochondrial cytochrome *c*

Mitochondrial cytochrome *c* (cyt *c*, hereafter) is a small soluble monomeric protein that contains a covalently bound c-type heme (Fig. 4A). The heme iron coordination is completed by His and Met axial ligands that provide a low spin nature to the metal center:  $S = 0$  in the reduced iron(II) form and  $S = 1/2$  in the oxidized iron(III) form.

With cyt *c* one goes further down by roughly another factor of 6 in molecular size and  $\tau_c$  (Fig. 1). For its small size and the low spin nature of the ferric form, oxidized cyt *c* has been one of the first paramagnetic molecules for which the solution structure has been solved by NMR [37–39], using homonuclear  $^1\text{H}$  two-dimensional (2D) NMR experiments only. Later on,  $^{15}\text{N}$ -labeling was introduced to measure backbone internal mobility via  $^{15}\text{N}$  longitudinal, transverse and rotating frame relaxation rates and  $^{15}\text{N}$ - $^1\text{H}$  NOE [40–42], as well as to take advantage of  $^1\text{H}$ - $^{15}\text{N}$  HSQC experiments for monitoring the interaction with small molecules [43] or other proteins via chemical shift perturbation mapping [44–46].  $^{15}\text{N}$ ,  $^{13}\text{C}$ -enrichment provides access to triple resonance experiments, which largely facilitate the task of sequence specific assignment for new cyt *c* variants [47], but are not strictly necessary given the low spectral complexity.

In cyt *c*, the reduced and oxidized forms interconvert with an exchange rate which is slow with respect to the chemical shift difference of the nuclei undergoing exchange; the magnetization transfer between the two species occurs and can be detected and quantified via the integrated intensity of cross peaks in two-dimensional exchange spectroscopy (EXSY) experiments, thus providing the chemical exchange rate constant. This self-exchange electron transfer process [48] has been traditionally determined via  $^1\text{H}$ - $^1\text{H}$  EXSY. A few years ago we have proposed homonuclear EXSY experiments relying on  $^{15}\text{N}$  or  $^{13}\text{C}$  as alternative and more robust tools [49,50]. Relevant to this contribution is the so-called COCO-EXSY experiment, where exchange between backbone carbonyl spins (here named CO) is observed. The experiment relies on the same pulse sequence as the  $^{13}\text{C}$ - $^{13}\text{C}$  NOESY, but in its EXSY version the mixing time is optimized to detect peaks arising from chemical exchange rather than dipolar interactions [49]. The resulting 2D spectrum is a homonuclear  $^{13}\text{C}'$  correlation (where  $\text{C}'$  indicates the backbone carbonyl carbon) in which, for each  $^{13}\text{C}'$  spin, the four-peak pattern typical of a homonuclear experiment with diagonal (self) peaks  $\text{C}'_{\text{ox}}\text{-C}'_{\text{ox}}$  and  $\text{C}'_{\text{red}}\text{-C}'_{\text{red}}$ , and cross (exchange) peaks  $\text{C}'_{\text{ox}}\text{-C}'_{\text{red}}$  and  $\text{C}'_{\text{red}}\text{-C}'_{\text{ox}}$  is observed.

Cyt *c* with  $^{13}\text{C}$ -enriched heme has also been used for  $^{13}\text{C}$ - $^{13}\text{C}$  NOESY and EXSY experiments, as it will be reviewed hereafter. These data are unpublished results from our laboratory.

While  $^{13}\text{C}$ -direct detection in its one-dimensional version has revealed to be useful for the observation of the resonances of axial ligands in high/intermediate spin iron(III) in hemeproteins [51–53], in the case of low spin iron(III) cyt *c*,  $^1\text{H}$  detection is sufficient to provide the signals of His18 and Met80, along with the proton resonances of the heme substituents [3,54]. Nevertheless, the use of  $^{13}\text{C}$ -enriched heme allows the assignment of core porphyrin resonances that provide useful

information about heme distortion and unpaired spin delocalization. In b-type heme proteins this type of information is retrieved by reconstruction with porphyrins  $^{13}\text{C}$ -labeled at selected positions and the spectral assignment substantially relies on the comparison of one-dimensional  $^{13}\text{C}$  spectra of differently labeled derivatives and/or on the use of  $^{13}\text{C}$ - $^{13}\text{C}$  incredible natural abundance double-quantum transfer experiment (INADEQUATE) or  $^1\text{H}$ - $^{13}\text{C}$ - $^{13}\text{C}$ -edited  $^1\text{H}$  double-resonance isotope-edited (DRIED) spectra [55–59]. In the case of cyt *c* the covalent linkage between two Cys residues (Cys14 and Cys17) and the heme does not allow a straightforward substitution of the heme cofactors with selectively labeled iron-porphyrins. Nevertheless, in our lab, fully  $^{13}\text{C}$ -enriched human cyt *c* was produced with reasonably good yield (about 4 mg/l) using  $^{13}\text{C}$ -glycerol as carbon source; no 2-mercaptoethane sulfonate (MESNA) and  $\delta$ -ALA were added to the media, but 100 mg/l  $\text{FeSO}_4$  were introduced to favor the heme synthesis. The one-dimensional  $^{13}\text{C}$  NMR spectra of fully  $^{13}\text{C}$ -enriched reduced and oxidized human cyt *c* are reported in Fig. 4B (top and middle panels, respectively). The spectrum of the iron(III) form displays several hyperfine shifted resonances between 220 and  $-80$  ppm, characterized by short  $T_1$  values; most of these resonances belong to the heme moiety, as indicated by their disappearance in the spectrum of the oxidized cyt *c* containing unlabeled heme (Fig. 4B, bottom panel).

In ferric cyt *c*, a  $^{13}\text{C}$ - $^{13}\text{C}$  NOESY spectrum with fast recycle delay and 75 ms mixing time was used to assign the core porphyrin  $^{13}\text{C}$  resonances (Fig. 4C and D) and to further confirm the assignment of protonated carbons of heme and axial ligand resonances. Cyt *c* is small and therefore has small  $\tau_c$  and relatively short  $T_1$  values (see Fig. 1), which are further decreased in the ferric form due to dipolar and contact contributions to paramagnetic relaxation [24]. The  $^{13}\text{C}$ - $^{13}\text{C}$  NOESY maps for a protein of this size are expected to provide only connectivities between  $^{13}\text{C}$ -nuclei at very short distances, typically those separated by a single bond, in agreement with our experimental findings, as summarized in Fig. 4D. Using  $^{13}\text{C}$ - $^{13}\text{C}$  EXSY spectra between the hyperfine shifted resonances of heme in ferric cyt *c* and the corresponding resonances of the ferrous form, we could fully assign also the porphyrin  $^{13}\text{C}$  resonances in the diamagnetic iron(II) cyt *c* (Fig. 4E).

Finally, using the pseudocontact shift for  $^1\text{H}_\text{N}$  and  $^{15}\text{N}_\text{H}$  of 76 non coordinating amino acids we derived the magnetic susceptibility anisotropy parameters, according to well-established procedures [37,39,60–62], and we back calculated the pseudocontact contributions for the porphyrin  $^{13}\text{C}$  (in the limit of the metal-centered approximation). By subtracting these values from the observed ones, we obtained an estimate of the contact shifts on the heme  $^{13}\text{C}$ , as summarized in Fig. 4C.

### 3. Conclusions

The idea behind this contribution is to provide the students of the Summer School and the readers some examples of the possible applications of an experiment which is easy to be acquired and interpreted. As shown for NikR, the  $^{13}\text{C}$ - $^{13}\text{C}$  NOESY can find applications as a fingerprinting method to obtain information on the presence/absence of multiple conformations in slow or semi-slow exchange on the NMR chemical shift time scale for amino acid side chains. It represents a facile tool for EXSY experiments when dealing with slow exchange phenomena (on the NMR chemical shift time scale) such as the self-exchange electron transfer process operative between the reduced and oxidized form of cyt *c*. It provides an efficient method to monitor the behavior of side chains when dealing with protein interactions with other macromolecules or (paramagnetic) metal ions. A good example of the latter application is provided by the identification of the binding area for the ferric species produced in ferritin. When applied to uniformly  $^{13}\text{C}$ -enriched porphyrins in recombinant heme proteins, the  $^{13}\text{C}$ - $^{13}\text{C}$  NOESY experiment is a valuable approach to derive information on the electronic structure of the heme iron.

Most importantly, the  $^{13}\text{C}$ - $^{13}\text{C}$  NOESY experiment is essentially the only tool for monitoring all amino acids side chains in solution experiments of very large molecular assemblies, as demonstrated for the homopolymeric 24-mer ferritin cage. The symmetry properties of the ferritin cage greatly simplify the spectra; heteropolymeric assemblies could be similarly studied by selective  $^{13}\text{C}$ -enrichment of a single type of subunits.

## Abbreviations

2D	two-dimensional
$\delta$ -ALA	$\delta$ -amino levulinic acid
CRINEPT	cross-correlated relaxation-enhanced polarization transfer
CRIPT	cross-correlated relaxation-induced polarization transfer
CSA	chemical shift anisotropy
Cyt c	cytochrome c
DRIED	double-resonance isotope-edited
EXSY	exchange spectroscopy
HSQC	heteronuclear single quantum correlation
INADEQUATE	incredible natural abundance double-quantum transfer experiment
MAS	magic angle spinning
MESNA	2-mercaptoethane sulfonate
NikR	nickel-dependent regulatory protein
NMRD	nuclear magnetic resonance dispersion
NOE	nuclear Overhauser effect
NOESY	nuclear Overhauser effect spectroscopy
$T_1$	longitudinal relaxation time
$T_2$	transverse relaxation time
TROSY	transverse relaxation-optimized spectroscopy
$\tau_c$	rotational correlation time

## Acknowledgements

The authors acknowledge the support and the use of resources of Instruct-ERIC, a Landmark ESFRI project, and specifically the CERM/CIRMMIP Italy Centre. VG is the recipient of a post-doctoral fellowship 2018 provided by Fondazione Veronesi.

## References

[1] I. Bertini, C. Luchinat, G. Parigi, E. Ravera, *NMR of Paramagnetic Molecules, Volume 2: Applications to Metallobiomolecules and Models*, 2nd edition, Elsevier Science, 2016.

[2] C. Luchinat, G. Parigi, E. Ravera, *Paramagnetism in Experimental Biomolecular NMR*, Royal Society of Chemistry, 2018.

[3] I. Bertini, P. Turano, A.J. Vila, Nuclear magnetic resonance of paramagnetic metalloproteins, *Chem. Rev.* 93 (1993) 2833–2932, <https://doi.org/10.1021/cr00024a009>.

[4] L. Banci, L. Bertini, C. Luchinat, *Nuclear and electron relaxation. The magnetic nucleus-unpaired electron coupling in solution*, VCH, Weinheim, New York, Basel, Cambridge, (1991).

[5] W. Bermel, I. Bertini, I.C. Felli, R. Kümmerle, R. Pierattelli, Novel  $^{13}\text{C}$  direct detection experiments, including extension to the third dimension, to perform the complete assignment of proteins, *J. Magn. Reson.* 178 (2006) 56–64, <https://doi.org/10.1016/j.jmr.2005.08.011>.

[6] W. Bermel, I. Bertini, L. Duma, I.C. Felli, L. Emsley, R. Pierattelli, P.R. Vasos, Complete assignment of heteronuclear protein resonances by protonless NMR spectroscopy, *Angew. Chem. Int. Ed. Eng.* 44 (2005) 3089–3092, <https://doi.org/10.1002/anie.200461794>.

[7] B.H. Oh, W.M. Westler, P. Darba, J.L. Markley, Protein carbon-13 spin systems by a single two-dimensional nuclear magnetic resonance experiment, *Science* 240 (1988) 908–911, <https://doi.org/10.1126/science.3129784>.

[8] W. Bermel, I. Bertini, I. Felli, M. Piccioli, R. Pierattelli,  $^{13}\text{C}$ -detected protonless NMR spectroscopy of proteins in solution, *Prog. Nucl. Magn. Reson. Spectrosc.* 48 (2006) 25–45, <https://doi.org/10.1016/j.pnmrs.2005.09.002>.

[9] I.C. Felli, R. Pierattelli,  $^{13}\text{C}$  direct detection NMR, *NMR of Biomolecules*, Wiley-Blackwell, 2012, pp. 432–443, <https://doi.org/10.1002/9783527644506.ch26>.

[10] W. Bermel, I. Bertini, I.C. Felli, R. Kümmerle, R. Pierattelli,  $^{13}\text{C}$  direct detection experiments on the paramagnetic oxidized monomeric copper, zinc superoxide dismutase, *J. Am. Chem. Soc.* 125 (2003) 16423–16429, <https://doi.org/10.1021/ja037676p>.

[11] R. Riek, J. Fiaux, E.B. Bertelsen, A.L. Horwich, K. Wuthrich, *Solution NMR*

*techniques for large molecular and supramolecular structures*, *J. Am. Chem. Soc.* 124 (2002) 12144–12153.

[12] G. Wider, NMR techniques used with very large biological macromolecules in solution, *Methods Enzymol.* 394 (2005) 382–398, [https://doi.org/10.1016/S0076-6879\(05\)94015-9](https://doi.org/10.1016/S0076-6879(05)94015-9).

[13] I. Bertini, I.C. Felli, R. Kümmerle, D. Moskau, R. Pierattelli,  $^{13}\text{C}$ - $^{13}\text{C}$  NOESY: an attractive alternative for studying large macromolecules, *J. Am. Chem. Soc.* 126 (2004) 464–465, <https://doi.org/10.1021/ja0357036>.

[14] R.R. Crichton, J.-P. Declercq, X-ray structures of ferritins and related proteins, *Biochim. Biophys. Acta* 1800 (2010) 706–718, <https://doi.org/10.1016/j.bbagen.2010.03.019>.

[15] D. Lalli, P. Turano, Solution and solid state NMR approaches to draw iron pathways in the ferritin nanocage, *Acc. Chem. Res.* 46 (2013) 2676–2685, <https://doi.org/10.1021/ar4000983>.

[16] C. Caillet-Saguy, M. Piccioli, P. Turano, N. Izadi-Pruneyre, M. Delepierre, I. Bertini, A. Lecroisey, Mapping the interaction between the hemophore HasA and its outer membrane receptor HasR using CRINEPT-TROSY NMR spectroscopy, *J. Am. Chem. Soc.* 131 (2009) 1736–1744, <https://doi.org/10.1021/ja804783x>.

[17] M. Sattler, S.W. Fesik, Use of deuterium labeling in NMR: overcoming a sizeable problem, *Structure* 4 (1996) 1245–1249, [https://doi.org/10.1016/S0969-2126\(96\)00133-5](https://doi.org/10.1016/S0969-2126(96)00133-5).

[18] H. Takagi, D. Shi, Y. Ha, N.M. Allewell, E.C. Theil, Localized unfolding at the junction of three ferritin subunits. A mechanism for iron release? *J. Biol. Chem.* 273 (1998) 18685–18688, <https://doi.org/10.1074/jbc.273.30.18685>.

[19] M. Matzapetakis, P. Turano, E.C. Theil, I. Bertini,  $^{13}\text{C}$ - $^{13}\text{C}$  NOESY spectra of a 480 kDa protein: solution NMR of ferritin, *J. Biomol. NMR* 38 (2007) 237–242, <https://doi.org/10.1007/s10858-007-9163-9>.

[20] P. Turano, D. Lalli, I.C. Felli, E.C. Theil, I. Bertini, NMR reveals pathway for ferric mineral precursors to the central cavity of ferritin, *Proc. Natl. Acad. Sci. U. S. A.* 107 (2010) 545–550, <https://doi.org/10.1073/pnas.0908082106>.

[21] E. Ravera, S. Ciambellotti, L. Cerofolini, T. Martelli, T. Kozyreva, C. Bernacchioni, S. Giuntini, M. Fragai, P. Turano, C. Luchinat, Solid-state NMR of PEGylated proteins, *Angew. Chem. Int. Ed. Eng.* 55 (2016) 2446–2449, <https://doi.org/10.1002/anie.201510148>.

[22] I. Bertini, F. Engelke, C. Luchinat, G. Parigi, E. Ravera, C. Rosa, P. Turano, NMR properties of sedimented solutes, *Phys. Chem. Chem. Phys.* 14 (2012) 439–447, <https://doi.org/10.1039/c1cp22978h>.

[23] I. Bertini, C. Luchinat, G. Parigi, E. Ravera, B. Reif, P. Turano, Solid-state NMR of proteins sedimented by ultracentrifugation, *Proc. Natl. Acad. Sci. U. S. A.* 108 (2011) 10396–10399, <https://doi.org/10.1073/pnas.1103854108>.

[24] M. Piccioli, P. Turano, Transient iron coordination sites in proteins: exploiting the dual nature of paramagnetic NMR, *Coord. Chem. Rev.* 284 (2015) 313–328, <https://doi.org/10.1016/j.ccr.2014.05.007>.

[25] C. Bernacchioni, C. Pozzi, F. Di Pisa, S. Mangani, P. Turano, Ferroxidase activity in eukaryotic ferritin is controlled by accessory-iron-binding sites in the catalytic cavity, *Chemistry* 22 (2016) 16213–16219, <https://doi.org/10.1002/chem.201602842>.

[26] C. Pozzi, F. Di Pisa, D. Lalli, C. Rosa, E. Theil, P. Turano, S. Mangani, Time-lapse anomalous X-ray diffraction shows how  $\text{Fe}(2+)$  substrate ions move through ferritin protein nanocages to oxidoreductase sites, *Acta Crystallogr. D Biol. Crystallogr.* 71 (2015) 941–953, <https://doi.org/10.1107/S1399004715002333>.

[27] C. Pozzi, F. Di Pisa, C. Bernacchioni, S. Ciambellotti, P. Turano, S. Mangani, Iron binding to human heavy-chain ferritin, *Acta Crystallogr. D Biol. Crystallogr.* 71 (2015) 1909–1920, <https://doi.org/10.1107/S1399004715013073>.

[28] I. Bertini, D. Lalli, S. Mangani, C. Pozzi, C. Rosa, E.C. Theil, P. Turano, Structural insights into the ferroxidase site of ferritins from higher eukaryotes, *J. Am. Chem. Soc.* 134 (2012) 6169–6176, <https://doi.org/10.1021/ja210084n>.

[29] F. Bou-Abdallah, G.C. Papaefthymiou, D.M. Scheswohl, S.D. Stanga, P. Arosio, N.D. Chasteen,  $\mu$ -1,2-Peroxo-bridged di-iron(III) dimer formation in human H-chain ferritin, *Biochem. J.* 364 (2002) 57–63, <https://doi.org/10.1042/bj3640057>.

[30] E.R. Bauminger, P.M. Harrison, D. Hechel, N.W. Hodson, I. Nowik, A. Treffy, S.J. Yewdall, Iron (II) oxidation and early intermediates of iron-core formation in recombinant human H-chain ferritin, *Biochem. J.* 296 (1993) 709–719, <https://doi.org/10.1042/bj2960709>.

[31] A.S. Pereira, P. Tavares, S.G. Lloyd, D. Danger, D.E. Edmondson, E.C. Theil, B.H. Huynh, Rapid and parallel formation of  $\text{Fe}^{3+}$  multimers, including a trimer, during H-type subunit ferritin mineralization, *Biochemistry* 36 (1997) 7917–7927, <https://doi.org/10.1021/bi970348f>.

[32] L. Banci, I. Bertini, F. Cantini, I.C. Felli, L. Gonnelli, N. Hadjilias, R. Pierattelli, A. Rosato, P. Voulgaris, The Atx1-Ccc2 complex is a metal-mediated protein-protein interaction, *Nat. Chem. Biol.* 2 (2006) 367–368, <https://doi.org/10.1038/nchembio797>.

[33] B. Zambelli, F. Musiani, S. Benini, S. Ciurli, Chemistry of  $\text{Ni}^{2+}$  in urease: sensing, trafficking, and catalysis, *Acc. Chem. Res.* 44 (2011) 520–530, <https://doi.org/10.1021/ar200041k>.

[34] F. Musiani, B. Bertoša, A. Magistrato, B. Zambelli, P. Turano, V. Losasso, C. Micheletti, S. Ciurli, P. Carloni, Computational study of the DNA-binding protein helicobacter pylori NikR: the role of  $\text{Ni}(2+)$ , *J. Chem. Theory Comput.* 6 (2010) 3503–3515, <https://doi.org/10.1021/ct900635z>.

[35] L. Mazzei, O. Dobrovolska, F. Musiani, B. Zambelli, S. Ciurli, On the interaction of *Helicobacter pylori* NikR, a Ni(II)-responsive transcription factor, with the urease operator: in solution and in silico studies, *J. Biol. Inorg. Chem.* 20 (2015) 1021–1037, <https://doi.org/10.1007/s00775-015-1284-0>.

[36] S. Benini, M. Cianci, S. Ciurli,  $\text{Ni}^{2+}$  *Helicobacter pylori* NikR contains four square-planar nickel-binding sites at physiological pH, *Dalton Trans.* 40 (2011) 7831–7833, <https://doi.org/10.1039/c1dt11107h>.

- [37] L. Banci, I. Bertini, H.B. Gray, C. Luchinat, T. Reddig, A. Rosato, P. Turano, Solution structure of oxidized horse heart cytochrome c, *Biochemistry* 36 (1997) 9867–9877, <https://doi.org/10.1021/bi970724w>.
- [38] L. Banci, I. Bertini, K.L. Bren, H.B. Gray, P. Sompornpisut, P. Turano, Solution structure of oxidized *Saccharomyces cerevisiae* iso-1-cytochrome c, *Biochemistry* 36 (1997) 8992–9001, <https://doi.org/10.1021/bi963025c>.
- [39] L. Banci, I. Bertini, K.L. Bren, H.B. Gray, P. Sompornpisut, P. Turano, Three-dimensional solution structure of the cyanide adduct of a Met80Ala variant of *Saccharomyces cerevisiae* iso-1-cytochrome c. Identification of ligand-residue interactions in the distal heme cavity, *Biochemistry* 34 (1995) 11385–11398, <https://doi.org/10.1021/bi00036a011>.
- [40] J.S. Fetrow, S.M. Baxter, Assignment of <sup>15</sup>N chemical shifts and <sup>15</sup>N relaxation measurements for oxidized and reduced iso-1-cytochrome c, *Biochemistry* 38 (1999) 4480–4492, <https://doi.org/10.1021/bi9827417>.
- [41] S.M. Baxter, J.S. Fetrow, Hydrogen exchange behavior of [U-<sup>15</sup>N]-labeled oxidized and reduced iso-1-cytochrome c, *Biochemistry* 38 (1999) 4493–4503, <https://doi.org/10.1021/bi982742z>.
- [42] P.D. Barker, I. Bertini, R. Del Conte, S.J. Ferguson, P. Hajieva, E. Tomlinson, P. Turano, M.S. Viezzoli, A further clue to understanding the mobility of mitochondrial yeast cytochrome c: a (<sup>15</sup>N) T<sub>1</sub>ρ investigation of the oxidized and reduced species, *Eur. J. Biochem.* 268 (2001) 4468–4476, <https://doi.org/10.1046/j.1432-1327.2001.02369.x>.
- [43] M. Assfalg, I. Bertini, R. Del Conte, A. Giachetti, P. Turano, Cytochrome c and organic molecules: solution structure of the p-aminophenol adduct, *Biochemistry* 46 (2007) 6232–6238, <https://doi.org/10.1021/bi7002857>.
- [44] I. Bertini, S. Chevance, R. Del Conte, D. Lalli, P. Turano, The anti-apoptotic Bcl-x(L) protein, a new piece in the puzzle of cytochrome c interactome, *PLoS One* 6 (2011) e18329, <https://doi.org/10.1371/journal.pone.0018329>.
- [45] B. Moreno-Beltrán, A. Díaz-Quintana, K. González-Arzola, A. Velázquez-Campoy, M.A. De la Rosa, I. Díaz-Moreno, Cytochrome c1 exhibits two binding sites for cytochrome c in plants, *Biochim. Biophys. Acta* 1837 (2014) 1717–1729, <https://doi.org/10.1016/j.bbabi.2014.07.017>.
- [46] K. Sakamoto, M. Kamiya, M. Imai, K. Shinzawa-Itoh, T. Uchida, K. Kawano, S. Yoshikawa, K. Ishimori, NMR basis for interprotein electron transfer gating between cytochrome c and cytochrome c oxidase, *Proc. Natl. Acad. Sci. U. S. A.* 108 (2011) 12271–12276, <https://doi.org/10.1073/pnas.1108320108>.
- [47] B. Moreno-Beltrán, A. Guerra-Castellano, A. Díaz-Quintana, R. Del Conte, S.M. García-Mauriño, S. Díaz-Moreno, K. González-Arzola, C. Santos-Ocaña, A. Velázquez-Campoy, M.A. De la Rosa, P. Turano, I. Díaz-Moreno, Structural basis of mitochondrial dysfunction in response to cytochrome c phosphorylation at tyrosine 48, *Proc. Natl. Acad. Sci. U. S. A.* 114 (2017) E3041–E3050, <https://doi.org/10.1073/pnas.1618008114>.
- [48] M.D. Liptak, R.D. Fagerlund, E.C. Ledgerwood, S.M. Wilbanks, K.L. Bren, The proapoptotic G41S mutation to human cytochrome c alters the heme electronic structure and increases the electron self-exchange rate, *J. Am. Chem. Soc.* 133 (2011) 1153–1155, <https://doi.org/10.1021/ja106328k>.
- [49] S. Cacciatore, M. Piccioli, P. Turano, Electron self-exchange of cytochrome c measured via <sup>13</sup>C detected protonless NMR, *J. Porphyrins Phthalocyanines* 17 (2012) 142–149, <https://doi.org/10.1142/S1088424612501404>.
- [50] S.C. Feifel, K.R. Stieger, A. Kapp, D. Weber, M. Allegrozzi, M. Piccioli, P. Turano, F. Lisdat, Insights into interprotein electron transfer of human cytochrome c variants arranged in multilayer architectures by means of an artificial silica nanoparticle matrix, *ACS Omega*. 1 (2016) 1058–1066, <https://doi.org/10.1021/acsomega.6b00213>.
- [51] C. Caillet-Saguy, M. Piccioli, P. Turano, G. Lukat-Rodgers, N. Wolff, K.R. Rodgers, N. Izadi-Pruneyre, M. Delepiere, A. Lecroisey, Role of the iron axial ligands of heme carrier HasA in heme uptake and release, *J. Biol. Chem.* 287 (2012) 26932–26943, <https://doi.org/10.1074/jbc.M112.366385>.
- [52] C. Caillet-Saguy, P. Turano, M. Piccioli, G.S. Lukat-Rodgers, M. Czjzek, B. Guigliarelli, N. Izadi-Pruneyre, K.R. Rodgers, M. Delepiere, A. Lecroisey, Deciphering the structural role of histidine 83 for heme binding in hemophore HasA, *J. Biol. Chem.* 283 (2008) 5960–5970, <https://doi.org/10.1074/jbc.M703795200>.
- [53] C. Caillet-Saguy, M. Delepiere, A. Lecroisey, I. Bertini, M. Piccioli, P. Turano, Direct-detected <sup>13</sup>C NMR to investigate the iron(III) hemophore HasA, *J. Am. Chem. Soc.* 128 (2006) 150–158, <https://doi.org/10.1021/ja054902h>.
- [54] L. Banci, I. Bertini, K.L. Bren, H.B. Gray, P. Turano, pH-dependent equilibria of yeast Met80Ala-iso-1-cytochrome c probed by NMR spectroscopy: a comparison with the wild-type protein, *Chem. Biol.* 2 (1995) 377–383, [https://doi.org/10.1016/1074-5521\(95\)90218-X](https://doi.org/10.1016/1074-5521(95)90218-X).
- [55] M. Rivera, G.A. Caignan, Recent developments in the <sup>13</sup>C NMR spectroscopic analysis of paramagnetic hemes and heme proteins, *Anal. Bioanal. Chem.* 378 (2004) 1464–1483, <https://doi.org/10.1007/s00216-003-2340-0>.
- [56] M. Rivera, F. Qiu, R.A. Bunce, R.E. Stark, Complete isomer-specific <sup>1</sup>H and <sup>13</sup>C NMR assignments of the heme resonances of rat liver outer mitochondrial membrane cytochrome b5, *J. Biol. Inorg. Chem.* 4 (1999) 87–98, <https://doi.org/10.1007/s007750050292>.
- [57] A.Y. Alontaga, R.A. Bunce, A. Wilks, M. Rivera, <sup>13</sup>C NMR spectroscopy of core heme carbons as a simple tool to elucidate the coordination state of ferric high-spin heme proteins, *Inorg. Chem.* 45 (2006) 8876–8881, <https://doi.org/10.1021/ic0607484>.
- [58] F. Qiu, M. Rivera, R.E. Stark, An <sup>1</sup>H-<sup>13</sup>C-<sup>13</sup>C-edited 1H NMR experiment for making resonance assignments in the active site of heme proteins, *J. Magn. Reson.* 130 (1998) 76–81, <https://doi.org/10.1006/jmre.1997.1276>.
- [59] M.J. Rodríguez-Marañón, F. Qiu, R.E. Stark, S.P. White, X. Zhang, S.I. Foundling, V. Rodríguez, C.L. Schilling, R.A. Bunce, M. Rivera, <sup>13</sup>C NMR spectroscopic and X-ray crystallographic study of the role played by mitochondrial cytochrome b5 heme propionates in the electrostatic binding to cytochrome c, *Biochemistry* 35 (1996) 16378–16390, <https://doi.org/10.1021/bi961895o>.
- [60] L. Banci, I. Bertini, K.L. Bren, M.A. Cremonini, H.B. Gray, C. Luchinat, P. Turano, The use of pseudocontact shifts to refine solution structures of paramagnetic metalloproteins: Met80Ala cyano-cytochrome c as an example, *JBIC*. 1 (1996) 117–126, <https://doi.org/10.1007/s007750050030>.
- [61] M. Assfalg, I. Bertini, P. Turano, A.G. Mauk, J.R. Winkler, H.B. Gray, <sup>15</sup>N-<sup>1</sup>H residual dipolar coupling analysis of native and alkaline-K79A *Saccharomyces cerevisiae* cytochrome c, *Biophys. J.* 84 (2003) 3917–3923, [https://doi.org/10.1016/S0006-3495\(03\)75119-4](https://doi.org/10.1016/S0006-3495(03)75119-4).
- [62] M. Assfalg, I. Bertini, A. Dolfi, P. Turano, A.G. Mauk, F.I. Rosell, H.B. Gray, Structural model for an alkaline form of ferricytochrome c, *J. Am. Chem. Soc.* 125 (2003) 2913–2922, <https://doi.org/10.1021/ja027180s>.